Rapid Three-Dimensional Velocimetry by Nuclear Magnetic Resonance Imaging

J. Andrew Derbyshire, Stephen J. Gibbs, T. Adrian Carpenter, and Laurance D. Hall
Herchel Smith Laboratory for Medicinal Chemistry, Cambridge University School of Clinical Medicine, Cambridge, CB2 2PZ England

The study of complex velocity fields has made substantial progress in recent years with the widespread implementation of laser doppler velocimetry (Durst et al., 1981). Together with classical techniques such as hot-wire anemometry (Lomas, 1986), these methods have provided means for studying both the spatial and temporal dependence of fluid velocities under a wide range of conditions including steady flow and turbulence. Unfortunately, there remain classes of systems for which existing methods may be prohibitively difficult to employ reliably: heterogeneous fluids such as pastes and slurries, and fluids bounded by geometries or materials which prevent conventional access to the volume of interest (for example, porous media). For both of these areas, magnetic resonance imaging (MRI) techniques offer a convenient means for discerning details of complex flows. One of the most important areas of application is blood flow *in vivo* in which even modest velocity resolution can provide very valuable information (Smith, 1990). Advances in MRI methodology and hardware now allow rapid and detailed flow imaging studies with both high spatial and high velocity resolution, and we present here both methods for and results of rapid, three-dimensional velocimetry by echo-planar MRI. The data acquisition speed, image spatial resolution, and velocity resolution attained not only represent benchmarks for magnetic resonance techniques, but also promise equally detailed measurements on previously inaccessible systems.

The flow sensitivity of magnetic resonance techniques has been exploited for many years (Suryan, 1951; Stejskal, 1965), and current practice has been recently reviewed (Smith, 1990; Caprihan and Fukushima, 1990). These techniques can be loosely categorized into magnitude and phase-based methods, which respectively exploit the magnitude and orientation of the local nuclear magnetization vector $\vec{M}$ as tags which can be monitored in both space and time. By imaging the local magnetization state after the creation and evolution of these tags, one can create images of the local displacements on the order of μm to cm occurring on a time scale of milliseconds to seconds.

Correspondence concerning this work should be addressed to L. D. Hall.

Equipment

Experimental data were acquired with an Oxford Research Systems Biospec I console and an Oxford Instruments 2T, 31-cm horizontal bore superconducting magnet. A home-built sine-spaced birdcage coil (Bolinger et al., 1989) was used for radio-frequency transmission and reception. A 10-cm-dia. Maxwell-Golay unshielded gradient set, with each coil driven by a series pair of Techron 7570 amplifiers, was used. Experimental data were transferred to Unix workstations for reconstruction, interpolation, and display.

Magnitude Methods: Two-Dimensional Tagged Imaging

A particularly graphic display of complex flow fields can be created directly by DANTE (Morris and Freeman, 1978) tagged MRI, in which the magnitude of the local magnetization is nulled in orthogonal sets of planes of the volume to be imaged. After a suitable evolution delay, during which time the nulled planes move with the local fluid velocity, the magnetization state is imaged (Axel and Dougherty, 1989; Mosher and Smith, 1990; Tyszka et al., 1991; Kose, 1992). If this process is repeated for two or more durations of the evolution delay, then local fluid displacements per unit time can be determined. Although rigorously tracking the tags is not trivial in practice, manual examination of the series of tagged images helps develop a qualitative appreciation of the general features of the velocity field in the region of interest.

A rapid and convenient imaging procedure for systems in which the NMR frequency distribution over the volume of interest can be made narrow is the echo-planar imaging (EPI) technique (Mansfield, 1977; Stehling et al., 1991), which typically permits two spatial dimensions to be encoded from a single excitation, allowing planar images of 64×64 pixels to be acquired in less than 100 ms.

The DANTE and EPI techniques can be readily combined, and Figure 1 shows examples of two-dimensional DANTE tagged EPI images of water flowing around two baffles fitted in a cylindrical tube. Figure 1a is a schematic of the baffle system studied. The images in Figure 1b are part of a series

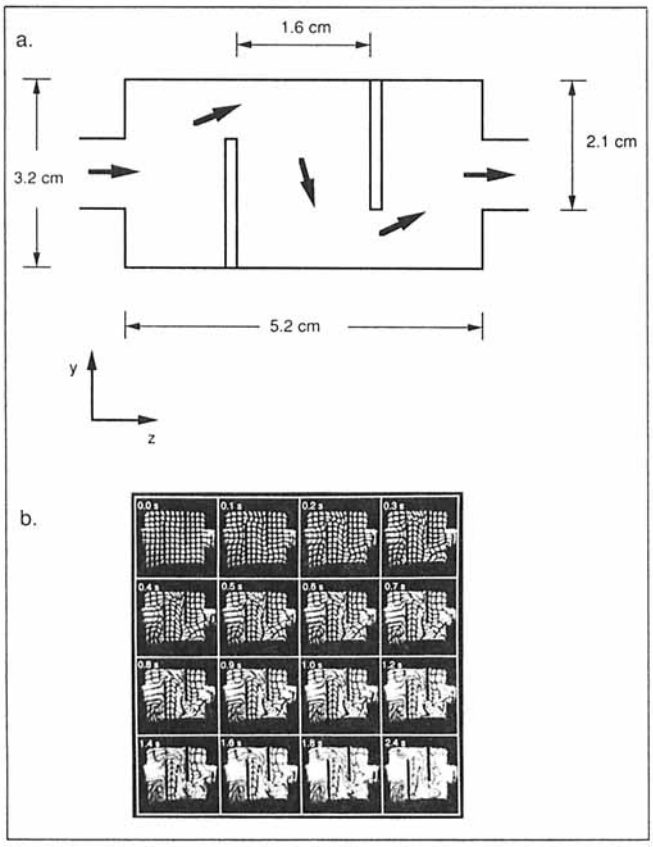

Figure 1a. Baffle geometry.

The phantom was machined from polymethylmethacrylate and filled with 1-mM $CuSO_4$ in distilled water.

Figure 1b. Two-dimensional DANTE tagged EPI images.

of 256 such images acquired in 20 min for different durations of the evolution delay T, the time between tagging and imaging, ranging from 0–2.55 s.

The DANTE tagged images of 1-mM $CuSO_4$ solution flowing through the baffle at a rate of 103-4 mL/min were obtained by inducing a grid pattern in the nuclear magnetization and allowing the distribution to evolve with the motion of the fluid for a variable time period, noted in the upper left corner of each image, before rapidly acquiring an image. Each of the two orthogonal sets of DANTE tags was created in 8 ms by irradiating the sample with a comb of rectangular radio-frequency pulses of 5.6-μs duration, at 500-μs intervals, in the presence of a magnetic field gradient. The pulse duration was chosen so that the selected tags would experience a full 90 degree excitation, and the field gradient in each tagging direction (Z and X) was adjusted to obtain 16 equally spaced tags across the image field of view. After tagging, the X gradient was left on for a further 1 ms to ensure dephasing of the tagged planes. In the first scan, no time was allowed for evolution of the spin distribution before image acquisition; in each successive experiment, the evolution delay was increased by 10 ms. Echo-planar images of 2-mm slice thickness and 64×64 pixel resolution covering a 7 cm (Z) $\times$ 5 cm (X) field of view were obtained in 50 ms under a 32 ms TE spin-echo envelope using a modified MBEST (Howseman et al., 1988) sequence. A set of 256 such images was obtained in about 20 min with a relaxation delay of 5 s between successive scans.

These images can be displayed in a moving picture fashion to obtain an excellent qualitative appreciation of the general features of the flow around the baffles. This type of result is useful in the early stages of an experimental investigation where only approximate results are required; for example, note in Figure 1b the recirculating region in the lower lefthand corner of the images and the relatively stagnant area to the right of both of the baffles.

Phase Methods: Three-Dimensional Velocity Imaging

More quantitative studies of the velocity field can be made by phase-based velocity sensitization methods, which encode in the phase of the local nuclear magnetization the displacement over a time interval Δ (Moran, 1982; Caprihan et al., 1990; Callaghan and Xia, 1991; Guilfoyle et al., 1991). The measured signal $A(\vec{r})$ from a voxel then has a dependency on translational motion given by:

$$A(\vec{r}) \approx \int_V A_0(\vec{r}) \exp\left[\Delta(i\vec{v}(\vec{r})\cdot\vec{k} - \vec{k}\cdot\boldsymbol{D}(\vec{r})\cdot\vec{k})\right]d\vec{r} \quad (1)$$

where $A_0(\vec{r})$ is a function of the local proton density and relaxation times, $\vec{v}(\vec{r})$ is the local fluid velocity, $\boldsymbol{D}(\vec{r})$ is the local intradiffusion tensor, $\vec{k}$ is a function of the magnitude and duration of phase encoding magnetic field gradient pulses used for motion encoding, and the integral is over the voxel volume. Hence, by performing experiments for several values of $\vec{k}$, the average velocities for each voxel may be determined. Modern frequency analysis methods are proving useful for this purpose (Kotyk et al., 1992).

Results of phase-encoded velocity imaging experiments obtained by a three-dimensional EPI technique are shown in Figure 2. These images were obtained by volume phase-encoding fluid displacement over a time interval $\Delta = 109$ ms with a stimulated echo pulse sequence (Gibbs et al., 1992; Bourgeois and Decorps, 1991) followed by longitudinal storage of magnetization. Three-dimensional imaging was then performed by an EPI sequence in combination with a phase-encoding magnetic field gradient (Z) orthogonal to the nominal imaging plane (XY). The 3D-EPI technique allows acquisition of a three-dimensional image of $64 \times 64 \times 64$ voxels in approximately 1 min (Johnson et al., 1983). Complex images were formed by adding data sets resulting from two acquisitions in which the phase of the storage radio-frequency pulse differed by 90 degrees. These images, corresponding to the phase angle of $A(\vec{r})$ in Eq. 1, can be instructive in themselves without need for further data processing; the ring structures in these images can be viewed as contours of $\vec{k}\cdot\vec{v}(\vec{r})\Delta$. The results shown are part of a set of 17 such images for the three Cartesian components of velocity, in which $|k|$ ranges from approximately 7 rad$\cdot$cm^{-1} to 1,200 rad$\cdot$cm^{-1}. The data were acquired in approximately 35 min for each complex image; four averages of each transient were acquired. The required time could be substantially reduced, probably by an order of magnitude, by many modifications: the implementation of shielded gradient coils; the use of a spin-echo rather than a stimulated echo for motion encoding; the acquisition of the echo directly rather

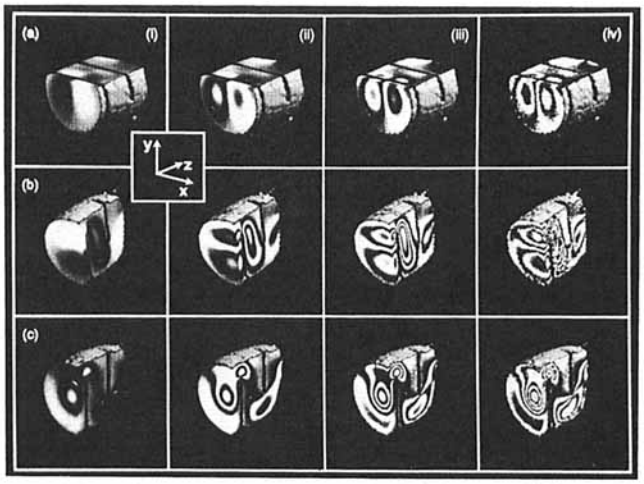

Figure 2. Flow-encoded 3-D NMR images.

Shown are 2-D projections of images of the local phase of the nuclear magnetization; a-c show images for selected values of $|\vec{k}| \approx$ (i) 140, (ii) 420, (iii) 710, and (iv) 990 rad·cm^{-1} along the x, y and z directions, respectively. The local phase in each of the images is proportional to $\vec{k} \cdot \vec{v}\Delta$, and hence the ring structures in these images can be viewed as contours of the relevant component of velocity; each corresponds to the condition that $\vec{k} \cdot \vec{v}\Delta$ is a constant.

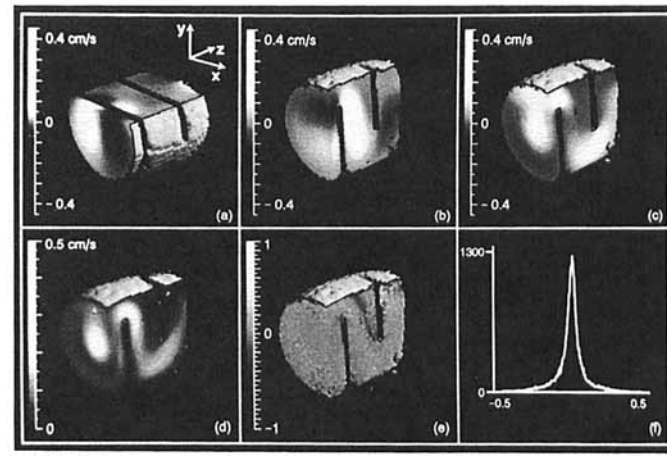

Figure 3. Three-dimensional velocity images.

These images show the individual velocity components as a function of position for the (a) x (b) y and (c) z components for a volumetric flow rate of 14 mL/min. (d) speed as computed from (a-c); (e) divergence of the velocity normalized by the local voxel turnover rate; (f) values of this normalized divergence.

than the storage and recall of one orthogonal component of the echo at a time; and optimization of the nuclear magnetic relaxation times of the fluid. The stimulated-echo method used here is robust and applicable to a wide variety of systems.

Frequency analysis of the three sets, one for each Cartesian component of velocity, of 17 of flow encoded images yields the velocity images in Figure 3. These results were obtained from the data in Figure 2 by zero-filling the three sets of 17 images to 512 points, Fourier transforming, and identifying the peaks in the resulting velocity spectra (approximately symmetric about the mean). Details such as the stagnation point and recirculation before the first baffle are readily apparent in these velocity images; further, the velocity component data can be manipulated to calculate, for example, a fluid speed image as shown in Figure 3d. Consistency of the data may be checked, for example, by calculating the divergence of the experimentally determined velocity. Figure 3e shows a map of the velocity divergence normalized with respect to the local voxel turnover rate. This normalized divergence represents the apparent fractional volume accumulation in a voxel in the time required to refresh the material in that volume. Nonzero values of the divergence may result from different systematic errors in each of the velocity component measurements or from imperfect spatial registration of the three data sets corresponding to the individual velocity components. The mean of the divergence of the velocity over the entire sampled volume is 2.1×10^{-4} s^{-1}, and the mean and standard deviation of the normalized divergence are -9.5×10^{-3} and 0.15, respectively, thus demonstrating that the velocity data satisfy local mass balances. The distribution of these local normalized divergence values [number of voxels vs. normalized divergence (dimensionless)] in Figure 3f demonstrates that the distribution of normalized divergence values is very peaked; the full width at half-maximum is approximately half of the standard deviation. The wide tails for this distribution might result from poor registration of the three velocity component images near boundaries.

Conclusions

The velocity and spatial resolution and accuracy obtained in the velocity component images in Figure 3 are expected to be adequate for checking the accuracy of model predictions for complex rheology. The acquisition speed attainable by EPI methods makes three-dimensional magnetic resonance imaging of velocity possible on a time scale of minutes to hours. These techniques are providing useful insight into the rheology of optically opaque fluids and into flow in opaque porous media (Guilfoyle et al., 1992). We expect that improvements in hardware and measurement protocols may allow equally detailed measurements for situations that are unsteady on a time scale of 100 ms (such as multiphase flow).

Acknowledgments

The authors thank Dr. Herchel Smith for an endowment which provided the facilities used and a studentship for JAD. SJG thanks both NATO and DTI-MAFF for financial support. The authors thank Dr. N. J. Herrod for providing image display software, and Cliff Bunch and Simon Smith for assistance with equipment.

Notation

A = NMR echo amplitude
A_0 = normalizing NMR echo amplitude
$\boldsymbol{D}$ = intradiffusion tensor
$\vec{k}$ = wave vector corresponding to the motion encoding magnetic field gradient pulses
$\vec{r}$ = position vector
T = evolution delay in DANTE tagged images
T_1 = longitudinal relaxation time for nuclear magnetization
T_2 = transverse relaxation time for nuclear magnetization
$\vec{v}$ = velocity
V = volume
Δ = time allowed for diffusion and flow
i = square root of -1

Literature Cited

Axel, L., and L. Dougherty, "MR Imaging of Motion with Spatial Modulation of Magnetization," *Radiology*, **171**, 841 (1989).

Bourgeois, D., and M. Decorps, "Quantitative Imaging of Slow Coherent Motion by Stimulated Echoes with Suppression of Stationary Water Signal," *J. Magn. Reson.*, **94**, 20 (1991).

Bolinger, L., M. G. Prammer, and G. S. Leigh, "A Multiple-Frequency Coil with a Highly Uniform B_1 Field," *J. Magn. Reson.*, **81**, 162 (1989).

Callaghan, P. T., and Y. Xia, "Velocity and Diffusion Imaging in Dynamic NMR Microscopy," *J. Magn. Reson.*, **91**, 326 (1991).

Caprihan, A., S. A. Altobelli, and E. Benitez-Read, "Flow-Velocity Imaging from Linear Regression of Phase Images with Techniques for Reducing Eddy-Current Effects," *J. Magn. Reson.*, **18**, 71 (1990).

Caprihan, A., and E. Fukushima, "Flow Measurements by NMR," *Phys. Reports*, **198**, 195 (1990).

Durst, F., A. Melling, and J. H. Whitelaw, *Principles and Practice of Laser-Doppler Anemometry*, 2nd ed., Academic Press, London (1981).

Gibbs, S. J., T. A. Carpenter, and L. D. Hall, "Diffusion Imaging with Unshielded Gradients," *J. Magn. Reson.*, **98**, 183 (1992).

Guilfoyle, D. N., P. Gibbs, R. J. Ordidge, and P. Mansfield, "Real-Time Flow Measurements Using Echo-Planar Imaging," *Magn. Reson. Med.*, **18**, 1 (1991).

Guilfoyle, D. N., P. Mansfield, and K. J. Packer, "Fluid Flow Measurement in Porous-Media by Echo-Planar Imaging," *J. Magn. Reson.*, **97**, 342 (1992).

Howseman, A. M., M. K. Stehling, B. Chapman, R. Coxon, R. Turner, R. J. Ordidge, M. G. Cawley, P. Glover, P. Mansfield, and R. E. Coupland, "Improvements in Snap-Shot Nuclear Magnetic-Resonance Imaging," *Br. J. Radiol.*, **61**, 822 (1988).

Johnson, G., J. M. S. Hutchinson, T. Redpath, and L. M. Eastwood, "Improvements in Performance Time for Simultaneous Three-Dimensional NMR Imaging," *J. Magn. Reson.*, **54**, 374 (1983).

Kose, K., "Visualization of Turbulent Motion Using Echo-Planar Imaging with a Spatial Tagging Sequence," *J. Magn. Reson.*, **98**, 599 (1992).

Kotyk, J. J., N. G. Hoffman, W. C. Hutton, G. L. Bretthorst, and J. J. H. Ackerman, "Comparison of Fourier and Bayesian Analysis of NMR Signals: I. Well-Separated Resonances (The Single-Frequency Case)," *J. Magn. Reson.*, **98**, 483 (1992).

Lomas, C. G., *Fundamentals of Hot-Wire Anemometry*, Cambridge University Press (1986).

Mansfield, P., "Multi-planar Image Formation Using NMR Spin Echoes," *J. Phys. C*, **10**, L55 (1977).

Moran, P. R., "A Flow Zeugmatotgraphic Interlace for NMR Imaging in Humans," *Magn. Reson. Imaging*, **1**, 197 (1982).

Morris, G. A., and R. Freeman, "Selective Excitation in Fourier Transform Nuclear Magnetic Resonance," *J. Magn. Reson.*, **29**, 433 (1978).

Mosher, T. J., and M. B. Smith, "A DANTE Tagging Sequence for the Evaluation of Translational Sample Motion," *Magn. Reson. Med.*, **15**, 334 (1990).

Smith, M. A., "The Measurement and Visualisation of Vessel Blood Flow by Magnetic Resonance Imaging," *Clin. Phys. Physiol. Meas.*, **11**, 101 (1990).

Stehling, M. K., R. Turner, and P. Mansfield, "Echo-Planar Imaging: Magnetic Resonance Imaging in a Fraction of a Second," *Sci.*, **254**, 43 (1991).

Stejskal, E. O., "Use of Spin Echoes in a Pulsed Magnetic Field Gradient to Study Anisotropic Restricted Diffusion and Flow," *J. Chem. Phys.*, **43**, 3597 (1965).

Suryan, G., "Nuclear Resonance in Flowing Liquids," *Proc. Indian Acad. Sci.*, **33**, 107 (1951).

Tyska, M., N. J. Shah, R. C. Hawkes, and L. D. Hall, "Visualization of Fluid Motion by Tagged Magnetic Resonance Imaging," *Flow Meas. Instrum.*, **2**, 127 (1991).

Manuscript received June 28, 1993, and revision received Sept. 9, 1993.